Editors' Suggestion

Artificial Atoms, Wigner Molecules, and an Emergent Kagome Lattice in Semiconductor Moiré Superlattices

Aidan P. Reddy, Trithep Devakul, and Liang Fu
Department of Physics, Massachusetts Institute of Technology, Cambridge, Massachusetts 02139, USA

(Received 20 January 2023; accepted 18 November 2023; published 14 December 2023)

Semiconductor moiré superlattices comprise an array of artificial atoms and provide a highly tunable platform for exploring novel electronic phases. We introduce a theoretical framework for studying moiré quantum matter that treats intra-moiré-atom interactions exactly and is controlled in the limit of large moiré period. We reveal an abundance of new physics arising from strong electron interactions when there are multiple electrons within a moiré unit cell. In particular, at filling factor $n = 3$, the Coulomb interaction within each three-electron moiré atom leads to a three-lobed "Wigner molecule." When their size is comparable to the moiré period, the Wigner molecules form an emergent Kagome lattice. Our Letter identifies two universal length scales characterizing the kinetic and interaction energies in moiré materials and demonstrates a rich phase diagram due to their interplay.

DOI: 10.1103/PhysRevLett.131.246501

Introduction.—The field of quantum science and engineering has long been fascinated with the creation of artificial atoms and artificial solids with desired properties. Artificial atoms, such as quantum dots and superconducting qubits, exhibit discrete energy levels and provide a physical carrier of quantum information. An array of coupled artificial atoms defines an artificial solid, which may be used for quantum simulation and quantum computing. Recently, the advent of moiré materials has provided a remarkably simple and robust realization of artificial solids, offering unprecedented opportunities to explore quantum phases of matter in two dimensions [1–3]. In particular, moiré superlattices of semiconductor transition metal dichalcogenides (TMDs) host strongly interacting electrons in a periodic potential. When the moiré period is large, doped electrons are spatially confined to the potential minima, leading to an array of artificial atoms. Electron tunneling between adjacent moiré atoms generates moiré bands. The charge density can be easily varied across a range of moiré band fillings by electrostatic gating, a means of manipulation unprecedented in natural solids whose electron density is determined by the chemistry of their constituent atoms. The *in situ* tunable atomic number in semiconductor moiré materials is a remarkable property.

To date, much theoretical analysis has relied on an effective Hubbard model description of interacting electrons in the lowest few moiré bands [4–7]. This approach successfully explains and predicts many observed phenomena such as the emergence of Mott insulators at $n = 1$ [8,9], incompressible Wigner crystals at fractional fillings $n < 1$ [8,10–17], and charge transfer between distinct species of moiré atoms at $n > 1$ [5,18–21] (n is the number of doped electrons or holes per moiré unit cell). However, it is important to note that the characteristic Coulomb interaction energy within a moiré atom is often several times larger than the single-particle superlattice gap. As a consequence, the low-energy Hilbert space can be substantially modified by interactions when multiple occupancy of moiré atoms is involved. An accurate many-body theory for semiconductor moiré systems therefore requires a proper treatment of the intra-moiré-atom interaction.

In this Letter, we predict new physics in semiconductor moiré systems arising from interaction effects at higher filling factors. We first develop an approach to modeling semiconductor moiré systems that treats the short-range electronic correlations within a single multielectron moiré atom exactly. We model each moiré atom as a potential well and solve the interacting few-electron atoms by exact diagonalization. Our approach is controlled in the "atomic limit" realized at large moiré period where electrons are tightly bound to moiré atoms and inter-atomic interactions can be neglected. For the three-electron atom (moiré lithium), we find a distinctive equilateral triangle Wigner molecule charge configuration [see Fig. 1(d)], which is stabilized by strong interaction and the threefold anisotropic moiré crystal field. We further show that when the Wigner molecules' size becomes comparable to the moiré period, they collectively form an emergent Kagome lattice of charges at filling factor $n = 3$ with electrons localized *between* moiré potential minima. This emergent Kagome lattice arises due to the balance between Coulomb interaction and moiré potential.

The change of charge configuration from triangular or honeycomb to Kagome lattice clearly demonstrates that the low-energy Hilbert space of moiré systems is strongly

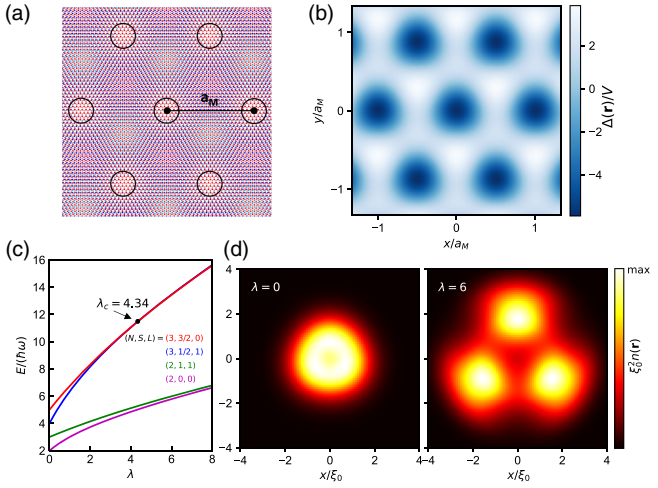

FIG. 1. Moiré atoms and Wigner molecules. (a) Schematic of moiré superlattice and (b) corresponding moiré potential at $\phi = 10°$. Its minima, moiré atoms, form a triangular lattice. (c) Evolution of each of the high- and low-spin ground states of harmonic helium and lithium (with two and three electrons respectively) with the Coulomb coupling constant λ. The overall ground state of harmonic lithium transitions from low to high spin at $\lambda_c = 4.34$. (d) Charge density distribution of the high spin ground state of moiré lithium including a crystal field corresponding to the continuum model parameters ($V = 15$ meV, $a_M = 14$ nm, $\phi = 10°$, $m = 0.5m_e$) without (left) and with (right) Coulomb interaction.

filling dependent due to interaction effects. Our Letter introduces parametrically controlled approximations for treating strong electron-electron interactions in semiconductor moiré superlattices and reveals striking consequences of the interplay between quantum kinetic, moiré potential, and Coulomb interaction energies.

Semiconductor moiré continuum model.—When two semiconductor TMD monolayers are stacked, a moiré pattern appears due to lattice mismatch and/or twist angle. When the moiré period a_M is much larger than the monolayer lattice constant, the single-particle moiré band structure is accurately described by a continuum model consisting of an effective mass approximation to the semiconductor band edge and a slowly varying effective periodic potential arising from band edge modulation throughout the moiré unit cell. In this Letter, we always refer to the doped carriers as electrons, regardless of the true sign of their charge. The continuum model Hamiltonian for TMD heterobilayers [4] (such as WSe_2/WS_2 and $MoSe_2/WSe_2$) and twisted Γ-valley homobilayers [22,23] (such as twisted MoS_2) assumes the form

$$\mathcal{H} = \frac{\boldsymbol{p}^2}{2m} + \Delta(\boldsymbol{r}) \tag{1}$$

where $\Delta(\boldsymbol{r}) = -2V\sum_{i=1}^{3}\cos(\boldsymbol{g}_i\cdot\boldsymbol{r} + \phi)$ is an effective moiré potential that has the translation symmetry of the superlattice in the first harmonic approximation, m is the effective mass, and $\boldsymbol{g}_i = (4\pi/\sqrt{3}a_M)[\sin(2\pi i/3), \cos(2\pi i/3)]$ are the moiré reciprocal lattice vectors [Fig. 1(a)]. The minima of $\Delta(\boldsymbol{r})$ define a periodic array of moiré atoms to which doped charge is tightly bound in the atomic limit which we now examine.

Moiré atoms.—We define an effective Hamiltonian for an electron confined to a moiré atom by Taylor expanding $\Delta(\boldsymbol{r})$ about the origin:

$$\Delta(\boldsymbol{r}) \approx \text{const} + \frac{1}{2}kr^2 + c_3\sin(3\theta)r^3 + \ldots \tag{2}$$

where $k = 16\pi^2 V\cos(\phi)/a_M^2$ and $c_3 = 16\pi^3 V\sin(\phi)/(3^{3/2}a_M^3)$. The result is a circular oscillator with frequency $\omega = \sqrt{k/m}$ along with higher-order, rotation-symmetry-breaking corrections, which we call the moiré crystal field. The effective Hamiltonian of an N-electron moiré atom includes a Coulomb interaction $e^2/(\epsilon|\boldsymbol{r}_i - \boldsymbol{r}_j|)$ between all of its electron pairs.

Both kinetic energy and Coulomb energy favor charge delocalization, whereas the confinement potential favors localization. The characteristic length $\xi_0 \equiv [\hbar^2/(mk)]^{1/4}$ at which the potential and kinetic energies of a harmonically confined electron are equal defines the size of a single-electron moiré atom (that is, the extent of its ground state wave function). We further introduce the length scale at which the Coulomb and confinement energies of two classical point charges arranged symmetrically about the origin of a harmonic potential are equal, $\xi_c = (e^2/2\epsilon k)^{1/3}$. The ratio of these two length scales is directly related to the dimensionless coupling constant that is the ratio of the intra-atomic Coulomb energy to the atomic level spacing: $\lambda \equiv [(e^2/\epsilon\xi_0)/\hbar\omega] = 2(\xi_c/\xi_0)^3$.

Importantly, the size of the ground state of a few-electron moiré atom, which we denote as ξ, is on the order of ξ_0 for $\lambda \ll 1$ (weak interaction) and ξ_c for $\lambda \gg 1$ (strong interaction), respectively. Therefore for general λ, we have $\xi \sim \max\{\xi_0, \xi_c\}$.

Importantly, we observe that the effective spring constant weakens with increasing moiré period: $k \propto a_M^{-2}$. It thus follows that

$$\xi_0 \equiv \left(\frac{\hbar^2}{mk}\right)^{1/4} \propto a_M^{1/2}; \qquad \xi_c \equiv \left(\frac{e^2}{2\epsilon k}\right)^{1/3} \propto a_M^{2/3}. \tag{3}$$

Consequently, at sufficiently large a_M, the hierarchy of length scales $a_M > \xi_c > \xi_0$ is necessarily realized. Then, the size of the few-electron moiré atom ξ is parametrically smaller than the distance between adjacent atoms a_M so that intra-atomic Coulomb interaction $\sim e^2/\xi$ dominates over inter-atomic interaction $\sim e^2/a_M$. This self-consistently justifies our treatment of isolated moiré atoms as the first step to understanding moiré solids. To ground our analysis, we plot the length scales ξ_c, ξ_0 and the coupling constant λ

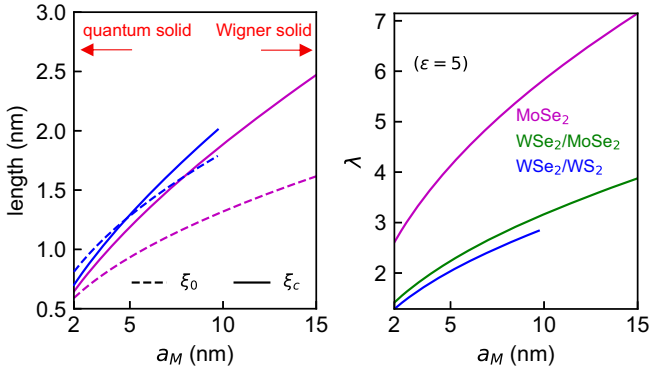

FIG. 2. Key parameters for TMD moiré heterostructures. Length scales ξ_0, ξ_c (left) and coupling constant λ (right) in the valence bands of several semiconductor moiré systems calculated according to continuum model parameters extracted from density functional theory [5,22,24].

as a function of the moiré period a_M for three representative TMD heterostructures in Fig. 2.

We begin by modeling each moiré atom as purely harmonic, neglecting the influence of the crystal field. The single-particle eigenstates of the circular oscillator are labeled by radial and angular momentum quantum numbers n and l with energy $E = (2n + |l| + 1)\hbar\omega$. We identify $N = 2n + |l| + 1$ as the principal quantum number and refer to the circular oscillator eigenstates using electron configuration notation accordingly (i.e. s for $l = 0$ and p for $|l| = 1$ states).

It is known rigorously that the ground state of two electrons with a time-reversal-symmetric Hamiltonian including a symmetric two-body interaction in arbitrary spatial dimensions is a spin singlet [25]. For all interaction strengths, the harmonic helium singlet ground state remains adiabatically connected to the $1s^2$, single-Slater-determinant ground state at $\lambda = 0$, and the triplet first-excited state to the $1s^1 2p^1$ state (see Fig. 1). Although the triplet-singlet energy gap remains positive for all λ, it asymptotically approaches 0 in the classical limit $\lambda \to \infty$.

The above theorem does not apply to systems of more than two electrons. In the absence of a Coulomb interaction and moiré crystal field, the moiré lithium ground state configuration is a $1s^2 2p$ spin doublet with total spin and angular momentum quantum numbers $(S, L) = (1/2, 1)$. At a critical coupling constant $\lambda_c \approx 4.34$, we find that a ground state level crossing occurs between this low-spin doublet and a high-spin quartet state with $(S, L) = (3/2, 0)$ originating from a $1s^1 2p^2$ configuration (see Fig. 1) [26,27]. After the level crossing, the energy difference between the low- and high-spin ground states remains small and asymptotes to 0 in the classical limit $\lambda \to \infty$. Since the energy splittings between the low- and high-spin ground states of the two- and three-electron moiré atoms are small, it should be possible to induce first-order spin transitions with a modest magnetic field [24,28,29].

The classical ground state of three interacting electrons in a harmonic potential is an equilateral triangle of side length $\xi_T = (2/\sqrt{3})^{1/3}\xi_c$ centered about the origin that spontaneously breaks rotational symmetry, a configuration which we refer to as a trimer. At finite λ, quantum fluctuation restores rotational symmetry while preserving the density-density correlations of the electron trimer [27]. On the other hand, the moiré crystal field term $\sin(3\theta)r^3$ breaks the rotational symmetry explicitly. Since the three-fold crystal anisotropy matches with the symmetry of the classical ground state, it stabilizes the triangular "Wigner molecule" in the presence of a Coulomb interaction. As we show in Fig. 1(c), the charge density of the $(N, S) = (3, 3/2)$ state in the absence of the Coulomb interaction ($\lambda = 0$) is distorted only mildly by the crystal field, whereas, at $\lambda = 6$, it develops a local minimum at the origin and three distinct lobes at the corners of an equilateral triangle. The low-spin state $S = 1/2$ exhibits a similar density profile in the presence of the crystal field at moderate and large λ (see Supplemental Material), again in agreement with the classical limit where spin plays no role. The unique charge distribution of the Wigner molecule is a clear consequence of strong interactions and can be directly observed via a local probe such as scanning tunneling microscopy [30].

A heuristic argument for the high-spin $S = 3/2$ ground state is that, in the semiclassical expansion, three-particle exchange processes dominate over two-particle exchange processes since the latter must overcome a large Coulomb energy barrier associated with relative coordinates whereas the former need not. Because three-particle exchange amplitudes are necessarily ferromagnetic [31,32], the ground state at large coupling constant should be fully spin polarized.

Moiré solids.—Having established the physics of isolated moiré atoms, we now turn to their crystalline ensembles: moiré solids. We reiterate the important observation that the hierarchy of length scales $a_M > \xi_c > \xi_0$ is necessarily realized at sufficiently large a_M. Equivalently, the energy scale of the moiré potential depth V necessarily dominates over inter- and intra-atom Coulomb energies e^2/a_M, e^2/ξ as well as the quantum zero-point energy $\hbar\omega \propto a_M^{-1}$ associated with harmonic confinement. As a result, the ground state in this regime at integer filling n is an insulating array of n-electron moiré atoms located at the moiré potential minima, which is adiabatically connected to the decoupled limit $a_M \to \infty$. In this regard, we note that insulating states at integer fillings up to $n = 8$ have been observed in the conduction band of an $MoSe_2/WS_2$ moiré superlattice [33].

In the following, we investigate the intermediate regime $a_M \sim \xi_c > \xi_0$ and reveal new physics that emerges from inter-atom coupling. We apply self-consistent Hartree-Fock theory to the continuum model [Eq. (1)] [34–36], which treats intra- and inter-atomic interactions on equal footing and accounts for the full periodic moiré potential. Our

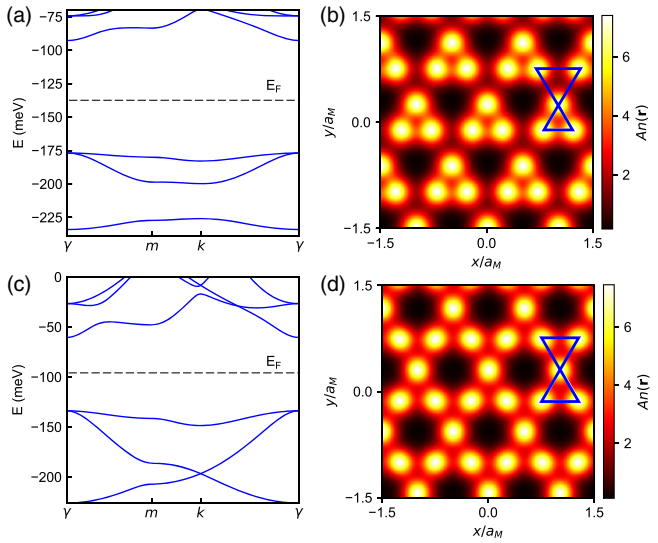

FIG. 3. Emergent Kagome lattice at $\mathbf{n} = \mathbf{3}$. (a) Quasiparticle band structure of self-consistent Hartree-Fock ground state with charge and spin density quantum numbers $(n, s_z) = (3, 3/2)$, resembling a Kagome lattice with broken inversion symmetry, i.e. a breathing Kagome lattice. Here we show only the spin-↑ bands. (b) Corresponding real space electron density, exhibiting peaks that approximately form a Kagome lattice. A is the moiré unit cell area. The parameters used are $V = 15$ meV, $\phi = 30°$, $m = 0.5m_e$, $a_M = 8$ nm, and $\epsilon = 5$. (c),(d) Results for $\phi = 60°$ where the continuum model is D_6 symmetric and a perfect Kagome lattice emerges at $n = 3$. Blue triangles in (b) and (d) indicate triangular Kagome plaquettes.

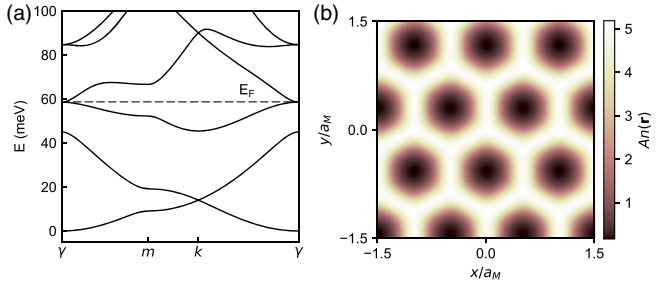

FIG. 4. Noninteracting bands. Noninteracting band structure and charge density at $n = 3$ for continuum model parameters ($V = 15$ meV, $\phi = 60°$, $m = 0.5m_e$, $a_M = 8$ nm, $\epsilon = 5$), which contrasts sharply with the interacting case shown in Figs. 3(c) and 3(d).

Hartree-Fock calculation, including the direct inversion of the iterative subspace convergence acceleration method, is detailed in the Supplemental Material [37]. In particular, at filling factor $n = 3$, we find that for realistic model parameters, electrons self-organize into an emergent Kagome lattice (Fig. 3). This interaction-induced charge order is particularly striking, given that the Kagome lattice sites where electrons localize are saddle points rather than minima of the moiré potential.

The origin of the emergent Kagome lattice can be understood in the regime $\xi_0 \ll \xi_c$ and a_M, which is smoothly connected to the classical limit $\xi_0 \to 0$ or equivalently $m \to \infty$. In this regime, the ground state is determined by the competition between the moiré potential and the Coulomb repulsion, which is controlled by the ratio a_M/ξ_c. As previously discussed, the ground state at large a_M/ξ_c is a lattice of electron trimers of size ξ_c separated by a distance of a_M. This charge configuration, which consists of upper and lower triangles of size $\sim\xi_c$ and a_M respectively, can be viewed as a precursor to the Kagome moiré solid. As a_M/ξ_c is reduced, the asymmetry in the size of the upper and lower triangles is naturally reduced, so that the charge configuration evolves toward the Kagome lattice.

Our Hartree-Fock calculations fully support the above picture. For generic ϕ, due to the lack of D_6 symmetry, the upper and lower triangles are distinct [Fig. 3(b)], thus realizing a breathing Kagome lattice. Indeed, the corresponding quasiparticle band structure, Fig. 3(a), resembles the Kagome lattice dispersion with broken inversion symmetry. As we show explicitly (see Supplemental Material [37]), the three lowest quasiparticle bands are adiabatically connected to the s and p_x, p_y bands on a triangular lattice (as evidenced by the twofold degeneracy at the γ point). This fully agrees with our picture of a Wigner molecule array evolving into a breathing Kagome lattice.

Even more interesting is the case $\phi = 60°$ as realized in twisted Γ valley TMD homobilayers. Here, the underlying moiré potential has two degenerate minima per unit cell forming a honeycomb lattice with D_6 symmetry. At the filling factor $n = 3$, our Hartree-Fock calculation finds that charge assembles into a perfectly symmetric Kagome lattice [Fig. 3(d)]. This is confirmed by the appearance of a Dirac point in the Hartree-Fock band structure [Fig. 3(c)]. Note that the Kagome band structure found here describes the dispersion of hole quasiparticles in the interaction-induced insulator at $n = 3$. In contrast, the noninteracting band structure at $\phi = 60°$, shown in Fig. 4, is gapless at this filling. In addition, the Kagome moiré solid features a symmetry-protected band degeneracy at γ below the Fermi level, which is absent in the noninteracting case.

It is interesting to note that the emergent Kagome lattice of charges minimizes neither the potential energy nor the Coulomb interaction energy. The potential energy favors charges localized at honeycomb lattice sites, while the Coulomb interaction favors a triangular lattice Wigner crystal. Yet, remarkably, our calculations demonstrate that the Kagome lattice emerges as a compromise due to their close competition for realistic material parameters.

Although our Hartree-Fock results shown in Fig. 3 are for fully spin-polarized electrons, the emergent Kagome insulator at $n = 3$ persists regardless of its spin configuration provided that ξ_c is comparable to a_M and sufficiently large compared to ξ_0. In this correlated insulating state,

the low energy degrees of freedom are localized spins whose coupling is an interesting problem that we leave to future study.

We now return to the key length scales and coupling constants of real semiconductor moiré systems shown in Fig. 2. As the coupling constant λ increases with a_M, the ground state at integer fillings evolves from a quantum solid where quantum effects dominate to a Wigner solid where classical effects dominate. In WSe_2/WS_2, the change between the two regimes corresponding to $\xi_c = \xi_0$ occurs around $a_M \sim 4.8$ nm. In twisted homobilayer $MoSe_2$, we find $\xi_c > \xi_0$ at all values of a_M shown, owing in part to its larger effective mass at the Γ valley [22,23]. Twisted Γ valley homobilayers (WS_2, MoS_2, and $MoSe_2$) also have moiré potentials with an emergent D_6 symmetry [22], making them ideal candidates to realize the emergent Kagome solid at small twist angle.

Our demonstration of the emergent Kagome lattice in TMD moiré heterostructures paves the way for future investigation of magnetic and topological phases it may host. The geometric frustration of antiferromagnetic Heisenberg model on the Kagome lattice makes it a promising candidate for quantum spin liquid [43–47]. The prospect that our emergent Kagome lattice may host such a phase deserves further investigation.

Summary.—Our Letter provides analytically controlled methods to treat strong interaction effect in moiré superlattices and reveals novel phases of matter at higher filling factors $n > 1$. We have identified three key length scales that universally govern the physics of all moiré materials: the moiré superlattice constant a_M, the quantum confinement length ξ_0, and crucially, the size of Wigner molecule ξ_c. ξ_0 characterizes the strength of quantum kinetic energy, and ξ_c the strength of Coulomb interaction.

We have established two parameter regions in which theoretical analysis is controlled even for strong interactions. First, when $a_M \gg \xi_0, \xi_c$, moiré atoms can be always treated in isolation regardless of the ratio ξ_c/ξ_0. By exactly solving the few-electron state of a single moiré atom, we have predicted the existence of the Wigner molecule. Second, when $\xi_0 \ll \xi_c, a_M$, a self-organized electron lattice is formed to minimize the sum of potential and interaction energy. In particular, we predict an emergent Kagome lattice at the filling $n = 3$ for realistic material parameters that correspond to $\xi_c \sim a_M$. More generally, when $\xi_0 \ll \xi_c$, the intra-atomic interaction $e^2/(\epsilon\xi_0)$ exceeds the single-particle band gap $\hbar\omega$, hence the effective Hamiltonian cannot be correctly obtained by projecting the interacting continuum model into the lowest moiré band. The interplay of the three length scales a_M, ξ_0, and ξ_c, in combination with tunable electron filling n, presents a vast phase space and an organizing principle to explore moiré quantum matter.

It is our pleasure to thank Yang Zhang, Faisal Alsallom, and Allan MacDonald for valuable discussions and related collaborations. This work was supported by the Air Force Office of Scientific Research (AFOSR) under Award No. FA9550-22-1-0432.

[1] Y. Cao, V. Fatemi, S. Fang, K. Watanabe, T. Taniguchi, E. Kaxiras, and P. Jarillo-Herrero, Unconventional superconductivity in magic-angle graphene superlattices, Nature (London) **556**, 43 (2018).

[2] E. Y. Andrei and A. H. MacDonald, Graphene bilayers with a twist, Nat. Mater. **19**, 1265 (2020).

[3] K. F. Mak and J. Shan, Semiconductor moiré materials, Nat. Nanotechnol. **17**, 686 (2022).

[4] F. Wu, T. Lovorn, E. Tutuc, and A. H. MacDonald, Hubbard model physics in transition metal dichalcogenide moiré bands, Phys. Rev. Lett. **121**, 026402 (2018).

[5] Y. Zhang, N. F. Q. Yuan, and L. Fu, Moiré quantum chemistry: Charge transfer in transition metal dichalcogenide superlattices, Phys. Rev. B **102**, 201115(R) (2020).

[6] J. Zang, J. Wang, J. Cano, and A. J. Millis, Hartree-Fock study of the moiré Hubbard model for twisted bilayer transition metal dichalcogenides, Phys. Rev. B **104**, 075150 (2021).

[7] N. Morales-Durán, N. C. Hu, P. Potasz, and A. H. MacDonald, Nonlocal interactions in moiré Hubbard systems, Phys. Rev. Lett. **128**, 217202 (2022).

[8] E. C. Regan, D. Wang, C. Jin, M. I. Bakti Utama, B. Gao, X. Wei, S. Zhao, W. Zhao, Z. Zhang, K. Yumigeta *et al.*, Mott and generalized Wigner crystal states in WSe_2/WS_2 moiré superlattices, Nature (London) **579**, 359 (2020).

[9] Y. Tang, L. Li, T. Li, Y. Xu, S. Liu, K. Barmak, K. Watanabe, T. Taniguchi, A. H. MacDonald, J. Shan *et al.*, Simulation of Hubbard model physics in WSe_2/WS_2 moiré superlattices, Nature (London) **579**, 353 (2020).

[10] Y. Xu, S. Liu, D. A. Rhodes, K. Watanabe, T. Taniguchi, J. Hone, V. Elser, K. F. Mak, and J. Shan, Correlated insulating states at fractional fillings of moiré superlattices, Nature (London) **587**, 214 (2020).

[11] H. Li, S. Li, E. C. Regan, D. Wang, W. Zhao, S. Kahn, K. Yumigeta, M. Blei, T. Taniguchi, K. Watanabe *et al.*, Imaging two-dimensional generalized Wigner crystals, Nature (London) **597**, 650 (2021).

[12] X. Huang, T. Wang, S. Miao, C. Wang, Z. Li, Z. Lian, T. Taniguchi, K. Watanabe, S. Okamoto, D. Xiao *et al.*, Correlated insulating states at fractional fillings of the WS_2/WSe_2 moiré lattice, Nat. Phys. **17**, 715 (2021).

[13] C. Jin, Z. Tao, T. Li, Y. Xu, Y. Tang, J. Zhu, S. Liu, K. Watanabe, T. Taniguchi, J. C. Hone *et al.*, Stripe phases in WSe_2/WS_2 moiré superlattices, Nat. Mater. **20**, 940 (2021).

[14] B. Padhi, R. Chitra, and P. W. Phillips, Generalized Wigner crystallization in moiré materials, Phys. Rev. B **103**, 125146 (2021).

[15] N. Morales-Durán, P. Potasz, and A. H. MacDonald, Magnetism and quantum melting in moiré-material Wigner crystals, Phys. Rev. B **107**, 235131 (2023).

[16] Y. Zhou, D. N. Sheng, and E.-A. Kim, Quantum phases of transition metal dichalcogenide moiré systems, Phys. Rev. Lett. **128**, 157602 (2022).

[17] B. A. Foutty, J. Yu, T. Devakul, C. R. Kometter, Y. Zhang, K. Watanabe, T. Taniguchi, L. Fu, and B. E. Feldman, Tunable spin and valley excitations of correlated insulators in γ-valley moiré bands, Nat. Mater. **22**, 731 (2023).

[18] K. Slagle and L. Fu, Charge transfer excitations, pair density waves, and superconductivity in moiré materials, Phys. Rev. B **102**, 235423 (2020).

[19] W. Zhao, B. Shen, Z. Tao, Z. Han, K. Kang, K. Watanabe, T. Taniguchi, K. F. Mak, and J. Shan, Gate-tunable heavy fermions in a moir'e Kondo lattice, Nature (London) **616**, 61 (2023).

[20] Y. Xu, K. Kang, K. Watanabe, T. Taniguchi, K. F. Mak, and J. Shan, A tunable bilayer Hubbard model in twisted WSe_2, Nat. Nanotechnol. **17**, 934 (2022).

[21] H. Park, J. Zhu, X. Wang, Y. Wang, W. Holtzmann, T. Taniguchi, K. Watanabe, J. Y. Yan, L. Fu, T. Cao, D. Xiao, D. R. Gamelin, H. Yu, W. Yao, and X. Xu, Dipole ladders with giant Hubbard u in a moiré exciton lattice (unpublished).

[22] M. Angeli and A. H. MacDonald, Γ valley transition metal dichalcogenide moiré bands, Proc. Natl. Acad. Sci. U.S.A. **118**, e2021826118 (2021).

[23] Y. Zhang, T. Liu, and L. Fu, Electronic structures, charge transfer, and charge order in twisted transition metal dichalcogenide bilayers, Phys. Rev. B **103**, 155142 (2021).

[24] C. R. Kometter, J. Yu, T. Devakul, A. P. Reddy, Y. Zhang, B. A. Foutty, K. Watanabe, T. Taniguchi, L. Fu, and B. E. Feldman, Hofstadter states and reentrant charge order in a semiconductor moir'e lattice, arXiv:2212.05068.

[25] E. Lieb and D. Mattis, Theory of ferromagnetism and the ordering of electronic energy levels, in *Inequalities* (Springer, New York, 2002), pp. 33–41.

[26] R. Egger, W. Häusler, C. H. Mak, and H. Grabert, Crossover from fermi liquid to Wigner molecule behavior in quantum dots, Phys. Rev. Lett. **82**, 3320 (1999).

[27] S. A. Mikhailov, Quantum-dot lithium in zero magnetic field: Electronic properties, thermodynamics, and fermi liquid–Wigner solid crossover in the ground state, Phys. Rev. B **65**, 115312 (2002).

[28] R. C. Ashoori, H. L. Stormer, J. S. Weiner, L. N. Pfeiffer, K. W. Baldwin, and K. W. West, *N*-electron ground state energies of a quantum dot in magnetic field, Phys. Rev. Lett. **71**, 613 (1993).

[29] M. Wagner, U. Merkt, and A. V. Chaplik, Spin-singlet–spin-triplet oscillations in quantum dots, Phys. Rev. B **45**, 1951 (1992).

[30] E. Wach, D. Żebrowski, and B. Szafran, Charge density mapping of strongly-correlated few-electron two-dimensional quantum dots by the scanning probe technique, J. Phys. Condens. Matter **25**, 335801 (2013).

[31] D. Thouless, Exchange in solid ^{3}He and the Heisenberg Hamiltonian, Proc. Phys. Soc. **86**, 893 (1965).

[32] K.-S. Kim, C. Murthy, A. Pandey, S. A. Kivelson, Interstitial-induced ferromagnetism in a two-dimensional Wigner crystal, Phys. Rev. Lett. **129**, 227202 (2022).

[33] T. Li, J. Zhu, Y. Tang, K. Watanabe, T. Taniguchi, V. Elser, J. Shan, and K. F. Mak, Charge-order-enhanced capacitance in semiconductor moiré superlattices, Nat. Nanotechnol. **16**, 1068 (2021).

[34] N. C. Hu and A. H. MacDonald, Competing magnetic states in transition metal dichalcogenide moiré materials, Phys. Rev. B **104**, 214403 (2021).

[35] Y.-M. Xie, C.-P. Zhang, J.-X. Hu, K. F. Mak, and K. T. Law, Valley-polarized quantum anomalous Hall state in moiré $MoTe_2/WSe_2$ heterobilayers, Phys. Rev. Lett. **128**, 026402 (2022).

[36] H. Pan, M. Xie, F. Wu, and S. Das Sarma, Topological phases in ab-stacked $MoTe_2/WSe_2$: Z_2 topological insulators, Chern insulators, and topological charge density waves, Phys. Rev. Lett. **129**, 056804 (2022).

[37] See Supplemental Material at http://link.aps.org/supplemental/10.1103/PhysRevLett.131.246501, which includes Refs. [38–42], for extended results and methodology.

[38] Y. Zeng and A. H. MacDonald, Strong modulation limit of excitons and trions in moiré materials, Phys. Rev. B **106**, 035115 (2022).

[39] A. Laturia, M. L. Van de Put, and W. G. Vandenberghe, Dielectric properties of hexagonal boron nitride and transition metal dichalcogenides: From monolayer to bulk, npj 2D Mater. Appl. **2**, 6 (2018).

[40] S. M. Reimann and M. Manninen, Electronic structure of quantum dots, Rev. Mod. Phys. **74**, 1283 (2002).

[41] G. Giuliani and G. Vignale, *Quantum Theory of the Electron Liquid* (Cambridge University Press, Cambridge, England, 2005).

[42] P. Pulay, Convergence acceleration of iterative sequences. The case of SCF iteration, Chem. Phys. Lett. **73**, 393 (1980).

[43] J.-W. Mei, J.-Y. Chen, H. He, and X.-G. Wen, Gapped spin liquid with Z_2 topological order for the kagome Heisenberg model, Phys. Rev. B **95**, 235107 (2017).

[44] P. Mendels and F. Bert, Quantum kagome frustrated antiferromagnets: One route to quantum spin liquids, C.R. Phys. **17**, 455 (2016).

[45] C. Broholm, R. Cava, S. Kivelson, D. Nocera, M. Norman, and T. Senthil, Quantum spin liquids, Science **367**, eaay0668 (2020).

[46] J. Motruk, D. Rossi, D. A. Abanin, and L. Rademaker, Kagome chiral spin liquid in transition metal dichalcogenide moiré bilayers, Phys. Rev. Res. **5**, L022049 (2023).

[47] D. Kiese, Y. He, C. Hickey, A. Rubio, and D. M. Kennes, TMDs as a platform for spin liquid physics: A strong coupling study of twisted bilayer WSe_2, APL Mater. **10**, 031113 (2022).